J|A|C|S
ARTICLES
Published on Web 08/19/2006

Room-Temperature Biosynthesis of Ferroelectric Barium Titanate Nanoparticles

Vipul Bansal,[†] Pankaj Poddar,[†] Absar Ahmad,[‡] and Murali Sastry*[,†,§]

Contribution from the Nanoscience Group, Materials Chemistry Division and Biochemical Sciences Division, National Chemical Laboratory, Pune - 411 008, India

Received May 1, 2006; E-mail: msastry@tatachemicals.com

Abstract: The syntheses of inorganic materials by biological systems is characterized by processes that occur close to ambient temperatures, pressures, and neutral pH, as is exemplified by biosilicification and biomineralization processes in nature. Conversely, laboratory-based syntheses of oxide materials often require extremes of temperature and pressure. We have shown here the extracellular, room-temperature biosynthesis of 4−5 nm ternary oxide nanoparticles such as barium titanate (BT) using a fungus-mediated approach. The tetragonality as well as a lowered Curie transition temperature in sub-10 nm particles was established, and the ferroelectricity in these particles was shown using Kelvin probe microscopy.

Introduction

$BaTiO_3$ (BT) is among the significant electroceramic dielectric materials of major interest for ferroelectric applications. BT has potential applications in nonvolatile memories, thin-film capacitors, pyroelectric detectors, infrared imaging systems, nonlinear optics, electrooptic modulators, optical memories, and microelectromechanical devices.[1−4] Barium titanate, particularly in its nanoparticulate form, has also recently found application as dielectric candidates for integration in the microelectronics industry.[2,5−7] However, further miniaturization of these devices is quite challenging as it is quite difficult to synthesize sub-10 nm BT particles of tetragonal symmetry and ferroelectric phase at room temperature. Most of the syntheses studies on BT thus far have reported existence of cubic and paraelectric phases at room temperature below a critical particle size.

By far the most commonly used processes for the syntheses of BT are conventional solid-state reactions and sol−gel techniques[8,9] that involve extreme temperature, pressure, and pH conditions. The development of soft-chemistry routes for the synthesis of $BaTiO_3$ nanocrystals has also started.[10−16] Recently, BT particles of 6−12 nm dimensions have been synthesized at room temperature (RT), using chemically synthesized complex peptide nanorings as a template.[17]

On the other hand, purely biological[18,19] and biomimetic[20,21] methods for the synthesis of oxide nanomaterials provide economically viable, environmentally benign, and energy-conserving processes. To the best of our knowledge, these biological and bioinspired methods have thus far been confined to the synthesis of binary oxide nanoparticles and have not been extended to the formation of complex ternary oxides such as barium titanate. We have recently shown that silica,[22,23] titania,[22] zirconia,[24] and magnetite[25] nanoparticles can be synthesized under ambient conditions utilizing the hydrolyzing capability of crude enzymes secreted by the plant pathogenic fungus *Fusarium oxysporum*. In this article, we show for the first time that a fungus may be used for the RT synthesis of ternary oxides such as barium titanate. Aqueous solutions of barium acetate and potassium hexafluorotitanate when reacted with

[†] Nanoscience Group, Materials Chemistry Division.
[‡] Biochemical Sciences Division.
[§] Current address: Tata Chemicals Ltd., Leela Business Park, Andheri-Kurla Road, Andheri (E), Mumbai, India.

(1) Bhalla, A. S.; Guo, R.; Roy, R. *Mater. Res. Innovations* **2000**, *4*, 3.
(2) Shaw, T. M.; McKinstry, S. T.; McIntyre, P.C. *Annu. Rev. Mater. Sci.* **2000**, *30*, 263.
(3) Cross, L. E.; McKinstry, S. T. *Encycl. Appl. Phys.* **1997**, *21*, 429.
(4) Lines, M. E.; Glass, A. M. *Principles and Applications of Ferroelectrics and Related Materials*; Oxford University Press: Oxford, 2001.
(5) Urban, J. J.; Spanier, J. E.; Lian, O. Y.; Yun, W. S.; Park, H. *Adv. Mater.* **2003**, *15*, 423.
(6) Naumov, I. I.; Bellaiche, L.; Fu, H. *Nature.* **2004**, *432*, 737.
(7) Fu, H. X.; Bellaiche, L. *Phys. Rev. Lett.* **2003**, *91*, 257601.
(8) Chandler, C. D.; Roger, C.; Hampden-Smith, M. J. *Chem. Rev.* **1993**, *93*, 1205.
(9) Veith, M.; Mathur, S.; Lecerf, N.; Huch, V.; Decker, T.; Beck, H. P.; Eiser, W.; Haberkorn, R. *J. Sol-Gel Sci. Technol.* **2000**, *17*, 145.
(10) Clark, I. J.; Takeuchi, T.; Ohtori, N.; Sinclair, D. C. *J. Mater. Chem.* **1999**, *1*, 83.
(11) Ciftci, E.; Rahaman, M. N.; Shumsky, M. *J. Mater. Sci.* **2001**, *36*, 4875.
(12) Walton, R. I.; Millange, F.; Smith, R. I.; Hansen, T. C.; O'Hare, D. *J. Am. Chem. Soc.* **2001**, *123*, 12547.
(13) Chen, H. J.; Chen, Y. W. *Ind. Eng. Chem. Res.* **2003**, *42*, 473.
(14) Niederberger, M.; Pinna, N.; Polleux, J.; Antonietti, M. *Angew. Chem., Int. Ed.* **2004**, *43*, 2270.
(15) Joshi, U. A.; Lee, J. S. *Small* **2001**, *1*, 1172.
(16) Garnweitner, G.; Hentschel, J.; Antonietti, M.; Niederberger, M. *Chem. Mater.* **2005**, *17*, 4594.
(17) Nuraje, N.; Su, K.; Haboosheh, A.; Samson, J.; Manning, E. P.; Yang, N.; Matsui, H. *Adv. Mater.* **2006**, *18*, 807.
(18) Shimizu, K.; Cha, J.; Stucky G. D.; Morse, D. E. *Proc. Natl. Acad. Sci. U.S.A.* **1998**, *95*, 6234.
(19) Kroger, N.; Deutzmann, R.; Bersdorf C.; Sumper, M. *Proc. Natl. Acad. Sci. U.S.A.* **2000**, *97*, 14133.
(20) Lovley, R.; Stolz, J. F.; Nord G. L.; Phillips, E. J. F. *Nature.* **1987**, *330*, 252.
(21) Patwardhan, S. V.; Mukherjee, N.; Steinitz-Kannan M.; Clarson, S. J. *Chem. Commun.* **2003**, *10*. 1122.
(22) Bansal, V.; Rautaray, D.; Bharde, A.; Ahire, K.; Sanyal, A.; Ahmad, A.; Sastry, M. *J. Mater. Chem.* **2005**, *15*, 2583.
(23) Bansal, V.; Sanyal, A.; Rautaray, D.; Ahmad, A.; Sastry, M. *Adv. Mater.* **2005**, *17*, 889.
(24) Bansal, V.; Rautaray, D.; Ahmad, A.; Sastry, M. *J. Mater. Chem.* **2004**, *14*, 3303.
(25) Bharde, A.; Rautaray, D.; Bansal, V.; Ahmad, A.; Sarkar, I.; Yusuf, S. M.; Sanyal, M.; Sastry, M. *Small* **2006**, *2*, 135.

10.1021/ja063011m CCC: $33.50

F. oxysporum resulted in the RT synthesis of nanocrystalline BT of 4−5 nm average size. These BT nanoparticles are ferroelectric and exhibit well-defined ferroelectric−paraelectric transition at room temperature. The ferroelectric behavior of the BT nanoparticles of such small dimensions has also been demonstrated using surface potential (Kelvin-probe) microscopy.

Experimental Section

The plant pathogenic fungus *Fusarium oxysporum* was cultured as described elsewhere.[26] The fungal mycelia was inoculated in a 500-mL Erlenmeyer flask containing 100 mL of MGYP medium and incubated for 72 h under shaking conditions (200 rpm) at 27 °C. After incubation, the fungal mycelia were harvested and washed thoroughly under sterile conditions. Twenty grams (wet weight) of the fungal biomass was then resuspended in 100 mL of aqueous solution containing a mixture of 10^{-3} M $(CH_3COO)_2Ba$ and 10^{-3} M K_2TiF_6 (Sigma-Aldrich Co., U.S.A.) in 500-mL Erlenmeyer flasks that were kept on a shaker (200 rpm) at 27 °C. Barium acetate was chosen as a source for Ba^{2+} ions since the acetate ions will act as energy source for the fungus and will be utilized during the fungal metabolism. Potassium hexafluorotitanate was chosen as a source for TiF_6^{2-} ions, which has been previously demonstrated by some of us to synthesize TiO_2 nanoparticles in the presence of fungi.[22] The reaction between the fungal biomass and the Ba^{2+} and TiF_6^{2-} ions was carried out for a period of 24 h. The biotransformed product was collected at the end of the reaction by separating the fungal mycelia from the aqueous extract through filtration. The barium titanate particles were precipitated by centrifugation at 10,000 rpm for 30 min after repeated washings with distilled water in order to remove the fungal extracellular proteins, unbound to BT particles. The BT particles were dried in air to form powder, and the powder was calcined at 400 °C for 2 h in order to degrade the proteins occluded within the particles aggregates during their synthesis.

The samples for transmission electron microscopy (TEM) and selected area electron diffraction (SAED) were prepared by drop coating onto a carbon-coated copper grid. SAED and TEM were performed on a JEOL 1200 EX instrument operated at an accelerating voltage of 120 kV while high-resolution TEM (HR-TEM) was performed on a JEOL JEM-2010 UHR instrument operated at a lattice image resolution of 0.14 nm. X-ray diffraction (XRD) measurements of films of the BT solutions drop-coated on glass substrates, were carried out on a Phillips PW 1830 instrument operated at a voltage of 40 kV and a current of 30 mA with Cu Kα radiation. The high-temperature wide-angle XRD (WAXD) measurements of BT powders were performed at 150 °C using Rigaku D_{max} 2500 wide-angle powder diffractometer with a diffracted beam graphite monochromator on a rotating anode generator with a Cu target.

A chemical analysis of BT nanoparticles was performed by X-ray photoemission spectroscopy (XPS). XPS measurements were carried out on the BT films cast on the Cu strips using a VG MicroTech ESCA 3000 instrument at a pressure $<1 \times 10^{-9}$ Torr and overall resolution of 1 eV. The general scan and Ba 3d, Ti 2p, and N 1s core-level spectra were recorded with nonmonochromatized Mg Kα radiation (photon energy = 1253.6 eV) at a pass energy of 50 eV and electron takeoff angle (angle between electron emission direction and surface plane) of 60°. The core-level spectra were background corrected using the Shirley algorithm,[27] and the chemically distinct species were resolved using a nonlinear least-squares fitting procedure. The core-level binding energies (BEs) were aligned with the adventitious carbon binding energy of 285 eV.

Differential scanning calorimentry (DSC) measurements of powders of as-synthesized and calcined BT nanoparticles were carried out on DSC-Q10 V9.0-275 instrument under nitrogen environment from 25 to 250 °C. For dielectric measurements, various percentages (0%, 2%, 10%, and 33% w/w) of calcined BT nanoparticles were dispersed in PMMA/chlorobenzene mixture and drop-casted onto glass substrates in the form of films. The solvent (chlorobenzene) was evaporated under vacuum, and the dried films were peeled off the glass substrate which were later cut into dimensions of 1 cm × 1 cm. The frequency and temperature-dependent dielectric response of these films were measured using a computer-controlled Solartron 1260 impedance analyzer.

Tapping mode surface potential microscopy (SPM) imaging of BT particles was performed using a NanoScope IV Multimode scanning probe microscope by VEECO Inc. For sample preparation, calcined BT nanoparticles dispersed in water were drop-coated directly onto AFM metallic packs mounted on a 6399e-piezoscanner (10 μm). For SPM imaging, 125-μm long metal-coated etched silicon probes were used. Topography, phase, and potential images were collected in the tapping mode at a scanning frequency of 1 Hz.

Results and Discussion

A representative TEM image of the BT nanoparticles obtained from the fungus *F. oxysporum* is shown in Figure 1A. The particles are of irregular quasi-spherical morphology with an average size of 4 ± 1 nm. The SAED analysis of the particle assemblies (inset, Figure 1A) clearly indicates that they are crystalline and the pattern could be indexed based on the tetragonal phase of barium titanate.[28] Figure 1B shows a representative TEM image of the BT nanoparticles after calcination at 400 °C for 2 h. Calcination of as-synthesized BT powder results in about 50% weight loss (up to 400 °C) due to decomposition of particle-bound biomacromolecules, as is evident from thermogravimetric analysis (TGA, curve 1, Supporting Information S1). After calcination, the BT nanoparticles become fairly regular in shape, with a slight increase in size ranging from 4−8 nm (Figure 1B). The SAED pattern of these particles indicates that they are also of the tetragonal phase (inset, Figure 1B).[28] Panels C and D of Figure 1 show HR-TEM images of calcined BT nanoparticles; the lattice planes exhibit a spacing of ∼2.88 Å (Figure 1C, (110) lattice planes) and ∼2.35 Å (Figure 1D, (111) lattice planes) of tetragonal BT. The previously reported lattice spacings for (110) and (111) lattice planes of bulk tetragonal BT correspond to 2.83 Å and 2.31 Å, respectively. The slight reduction in d-spacings in the biologically synthesized nanoparticles may be due to the lattice expansion.[29] We note that the particle shown in Figure 1C consists of a narrow twin boundary region. The fact that the

(26) Mukherjee, P.; Senapati, S.; Mandal, D.; Ahmad, A.; Khan, M. I.; Kumar R.; Sastry, M. *ChemBioChem* **2002**, *3*, 461.
(27) Shirley, D. A. *Phys. Rev. B* **1972**, *5*, 4709.
(28) Takeuchi, T.; Tabuchi, M.; Ado, K.; Honjo, K.; Nakamura, O.; Kageyama, H.; Suyama, Y.; Ohtori, N.; Nagasawa, M. *J. Mater. Sci.* **1997**, *32*, 4053.
(29) Tsunekawa, S.; Ito, S.; Mori, T.; Ishikawa, K.; Li, Z. Q.; Kawazoe, Y. *Phys. Rev. B* **2000**, *62*, 3065.

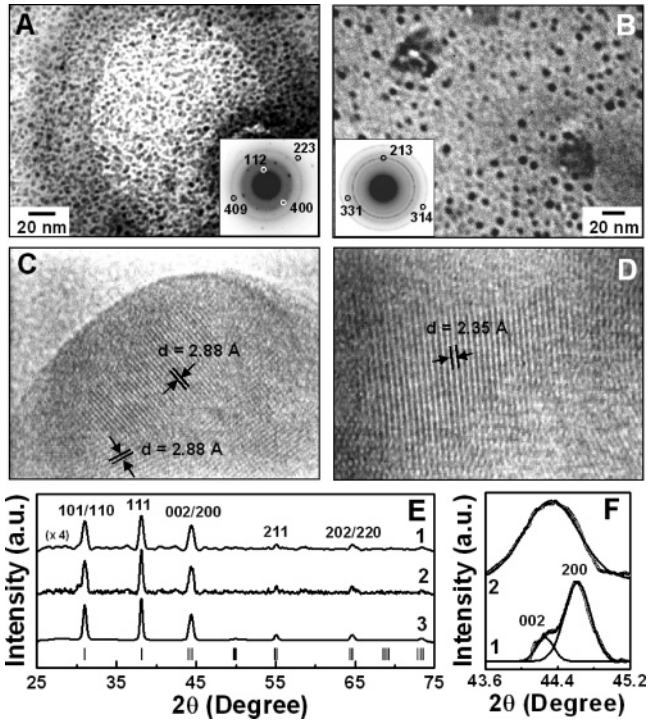

Figure 1. (A and B) TEM micrographs of BT nanoparticles synthesized using *F. oxysporum* before (A) and after (B) calcination at 400 °C for 2 h. The insets in A and B are SAED patterns recorded from representative BT particles. (C and D) HR-TEM images of BT nanoparticles after calcination. (E) XRD patterns of as-synthesized BT nanoparticles (curve 1), after calcination at 400 °C for 2 h (curve 2) and simulated diffraction pattern from calcined sample (curve 3). The intensity of curve 1 in E has been multiplied by a factor of 4 for reasons of clarity. (F) XRD patterns of calcined BT nanoparticles in the region of (002)/(200) diffraction planes at room temperature (curve 1) and at 150 °C (curve 2) The raw data are shown as dotted lines, while the Lorentzian fits of the curves are shown as solid lines.

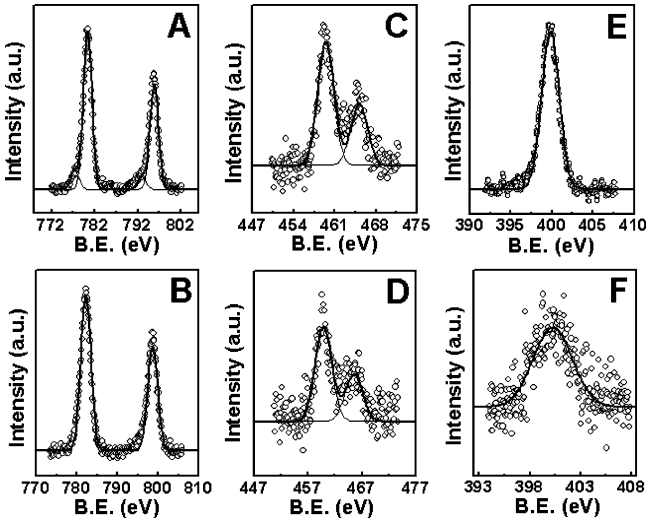

Figure 2. XPS data showing the Ba 3d (A and B), Ti 2p (C and D), and N 1s (E and F) core-level spectra recorded from as-synthesized (upper row) and calcined BT nanoparticles (lower row). The chemically resolved components are shown as solid lines in the figure and are discussed in the text.

capacitance of such a structure can be large has been put to use in boundary-layer capacitors made of polycrystalline BT.[30]

To further verify the deviation in lattice parameters for BT nanoparticles, XRD analysis of as-synthesized (curve 1, Figure 1E) as well as calcined BT nanoparticles (curve 2, Figure 1E) was done. The diffraction pattern obtained from the calcined BT nanoparticles (curve 2, Figure 1E) was subjected to Pauley's refinement (MS Modeling 3.0 software) assuming a c/a ratio of 1 (curve 3, Figure 1E). The lattice constants obtained were $a = b = 4.0810(7)$ Å and $c = 4.0992(6)$ Å and could be assigned to the $P4mm$ crystal structure of tetragonal symmetry with an R factor of 7.09%. The lattice spacings obtained from the simulated diffraction pattern for the (110) and (111) lattice planes are 2.88 Å and 2.35 Å, respectively (curve 3, Figure 1E) and match the lattice spacings observed in the HR-TEM images (Figure 1, C and D). In general, line broadening in X-ray powder diffraction measurements occurs in very small crystallites, which is generally a result of combined effects of the crystallite size, nonuniform strain, and instrumental broadening. Such a phenomenon acts as an obstacle for the structural characterization, particularly for $BaTi0_3$, with small tetragonality ($c/a = 1.004$). Hence, in order to provide a definite evidence for tetragonal/cubic transformation of BT particles, room-temperature as well as high-temperature XRD measurements in the region of the (002)/(200) Bragg reflections was performed at a slower scan rate of 0.25 deg/min. The XRD peak profiles in two cases were fitted with Lorentzian curves in order to separate the (002) and (200) components. The XRD pattern obtained at room temperature (curve 1, Figure 1F) showed the presence of an asymmetric peak (002)/(200) around $2\Theta = 45°$ which confirms tetragonal distortion in BT particles at room temperature. However, at 150 °C (above the Curie point of bulk BT), the XRD spectrum obtained (curve 2, Figure 1F) could only be fitted to a single Lorentzian component, thus indicating the presence of cubic phase above the Curie temperature (T_C). Hence, temperature-dependent XRD measurements provide clear evidence for tetragonal/cubic transformation in sub-10 nm BT particles.

Chemical analyses of as-synthesized and calcined BT nanoparticles were performed by XPS (Figure 2). The Ba 3d (Figure 2, A and B) and Ti 2p (Figure 2, C and D) core-level spectra from as-synthesized (Figure 2, A and C) as well as calcined (Figure 2, B and D) BT were recorded, which could be fitted into single spin−orbit pairs (spin−orbit splitting 15.4 eV for Ba and 5.7 eV for Ti)[31] with Ba $3d_{5/2}$ binding energies (BEs) of 779.7 eV (Figure 2, A and B) and Ti $2p_{3/2}$ BE of 458.5 eV (Figure 2, C and D). These values match closely with that of the previously reported nanocrystalline BT system.[29] In order to trace the proteins bound to BT nanoparticles, N 1s core-level spectra were also recorded from as-synthesized (Figure 2E) as well as calcined BT (Figure 2F), both of which could be fitted into single BE components of 400.3 eV, which matches closely with N 1s BE in amide bonds.[31] The presence of a low-intensity N 1s signature after calcination (Figure 2F) indicates the presence of capping proteins even in calcined BT particles that restrict the aggregation of calcined BT nanoparticles, as is clear from the TEM image of calcined BT (Figure 1B) and from weight loss observed in TGA of calcined BT (curve 2, Supporting Information S1). It is noteworthy that signatures of $BaCO_3$ were not observed in the XPS spectra, which is

(30) Bauer, C. L.; Seager, C. H. In *Solid State Physics Source Book*, 6th ed.; Parker, S. P., Ed.; McGraw-Hill Book Co.: New York, 1988.

(31) Wagner, C. D.; Riggs, W. M.; Davis, L. E.; Moulder J. F.; Muilenberg, G. E. *Handbook of X-ray Photoelectron Spectroscopy*; Perkin Elmer Corp. Publishers: Eden Prairie, MN, 1979.

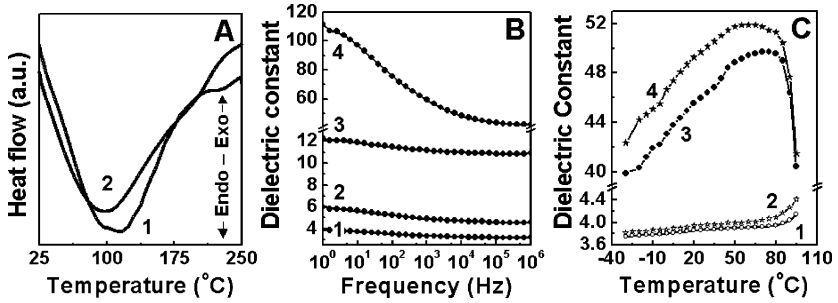

Figure 3. (A) DSC spectra recorded from BT nanoparticles synthesized using *F. oxysporum* before (curve 1) and after (curve 2) calcination at 400 °C for 2 h. (B) Frequency-dependent dielectric spectra recorded from PMMA (curve 1) and from PMMA embedded with 2% (curve 2), 10% (curve 3), and 33% (curve 4) of calcined BT nanoparticles. (C) Temperature-dependent dielectric spectra recorded from PMMA (curves 1 and 2) and 33% BT−PMMA nanocomposite (curves 3 and 4) at 10 kHz (curves 1 and 3) and 1 kHz (curves 2 and 4) respectively.

particularly significant considering the fact that $BaCO_3$ is the commonest impurity in BT synthesis system.

DSC measurements in the temperature range 25−250 °C were performed on as-synthesized and calcined BT powders (curves 1 and 2, respectively, Figure 3A). The as-synthesized BT nanoparticles show a broad exothermic/endothermic transition at 114 °C (curve 1, Figure 3A), whereas the calcined sample shows a similar broad transition at 98 °C, which is a signature of tetragonal to cubic transition. To our knowledge, such a transition has been observed for the first time for sub-10 nm sized particles. The marginally lower phase-transition temperature in comparison with bulk BT (∼128 °C) is due to reduction in BT particle size; this is known to reduce the transition temperature which is associated with ferroelectric to paraelectric phase transition.[32] This motivated us to study the frequency- and temperature-dependent dielectric properties of BT nanoparticles. For this purpose, various percentages (w/w) of BT nanoparticles (calcined at 400 °C for 2 h) were embedded in PMMA polymer and were casted in the form of free-standing films. These polymer composites as well as BT powders were also analyzed by Fourier transform infrared spectroscopy (FTIR, Supporting Information S2; Figure S2A) and tapping mode AFM (Supporting information S2, Figure S2, B and C).

Frequency-dependent dielectric measurements were performed at room temperature for a frequency sweep from 1 MHz to 1 Hz for various BT−PMMA composite films containing 0% (curve 1), 2% (curve 2), 10% (curve 3), and 33% (curve 4, percentages by weight) of BT (Figure 3B). A gradual increase in permittivity of BT−PMMA composite corresponding to an increase in BT content in PMMA from 0% to 33% is observed (curves 1−4, Figure 3B). The dielectric value obtained from pure PMMA, without any BT doping (curve 1, Figure 3B) matches closely with literature reports (∼2.6 at 1 MHz frequency).[33] The dielectric values of BT in BT−PMMA composite was calculated using Inverse Maxwell Garnett (MG) equation,[34] which is the most commonly used mixing formula explaining dielectric permittivities of composites, wherein ϵ_{eff} is the permittivity of BT−PMMA composite, ϵ_{i} is the permittivity of BT particles, ϵ_{e} is the permittivity of PMMA matrix and f is the fraction of BT in PMMA particles.

$$\epsilon_{\text{eff}} = \epsilon_{\text{i}} + 3(1-f)\epsilon_{\text{i}} \frac{\epsilon_{\text{e}} - \epsilon_{\text{i}}}{\epsilon_{\text{e}} + 2\epsilon_{\text{i}} - (1-f)(\epsilon_{\text{e}} - \epsilon_{\text{i}})}$$

The dielectric values calculated for BT using MG mixing formula at 1 MHz frequency were found to be 350−400. Although the dielectric values obtained on BT nanoparticles are much lower when compared to that of bulk BT,[35] this is consistent with the fact that one will expect a reduction of dielectric values on size reduction.[36] These results correlate well with the HR-TEM and XRD studies (Figure 1, C−E) that also exhibit the tetragonality in BT nanoparticles responsible for this ferroelectric behavior.

Temperature-dependent dielectric measurements were also performed on pure PMMA films (curves 1−2, Figure 3C) as well as on PMMA films containing 33% BT (curves 3−4, Figure 2C) between −35 °C and 100 °C at fixed frequencies of 10 kHz (curves 1 and 3, Figure 3C) and 1 kHz (curves 2 and 4, Figure 3C). Higher dielectric values were observed at 1 kHz as compared to those at 10 kHz (compare curves 2 and 4 with curves 1 and 3, respectively). In BT samples (curves 3 and 4, Figure 3C), we also observed a broad diversion in the dielectric constant with a maximum around 75 °C at 10 kHz (curve 3, Figure 3C) and a maximum around 65 °C at 1 kHz (curve 4, Figure 3C). It appears as if there is a reduction in Curie temperature with a reduction in the applied frequency. Moreover, a disparity in the T_C values obtained from temperature-dependent dielectric measurements at various frequencies (75 and 65 °C at 10 and 1 kHz, respectively) and those from DSC measurements (98 °C) (curve 2, Figure 3A) was also observed. Although broadening of peaks in DSC and dielectric measurements can be explained on the basis of size reduction of BT nanocrystallite, as observed previously,[37] the difference in T_C values under varying conditions cannot be explained solely on the basis of size effect. We believe that biologically synthesized BT particles are behaving as "ferroelectric relaxor" materials, since a broadening in the maxima of the temperature-dependent dielectric response as well as DSC maximum at ferroelectric transition is typical of "relaxor" materials, which are known to exhibit a diffused phase transition (DPT).[38] In addition, DPT is also characterized by frequency-dependent dispersion of dielectric constant, implying a frequency dependence of apparent T_C and a difference in the value of T_C obtained from different physical measurements.[38] Although pure BT, without any cationic

(32) Ma, Y.; Vileno, E.; Suib, S. L.; Dutta, P. K. *Chem. Mater.* **1997**, *9*, 3023.
(33) Neal, T. D.; Okamoto, K.; Scherer, A. *Opt. Express* **2005**, *13*, 5522.
(34) Sihvola, A. *Subsurf. Sens. Technol. Appl.* **2000**, *1*, 393.
(35) Frey, M. H.; Payne, D. A. *Chem. Mater.* **1995**, *7*, 123.
(36) Yashima, M.; Hoshina, T.; Ishimura, D.; Kobayashi, S.; Nakamura, W.; Tsurumi, T.; Wada, S. *J. Appl. Phys.* **2005**, *98*, 014313.
(37) Begg, B. D.; Vance, E. R.; Nowotny, J. *J. Am. Ceram. Soc.* **1994**, *77*, 3186.
(38) Chattopadhyay, S.; Ayyub, P.; Palkar, V. R.; Multani, M. *Phys. Rev. B* **1995**, *52*, 13177.

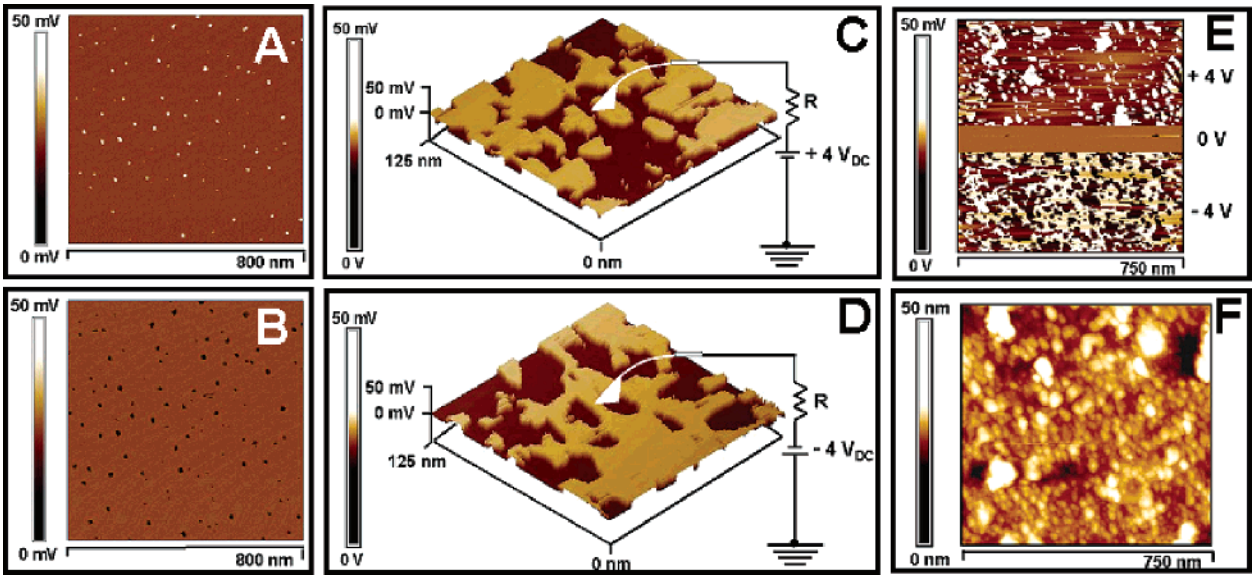

Figure 4. (A−D) Low magnification (A and B) and higher magnification (C and D) SPM images from BT particles obtained in potential mode after application of +4 V (A and C) and −4 V (B and D) external DC bias voltages respectively. (E and F) Potential image of BT particles obtained after sequential application of +4, 0, and −4 V external DC bias voltages to the conductive AFM tip (E) and height image of BT particles without any external bias voltage (F).

impurity, is not an excellent ferroelectric relaxor, a few reports exist wherein the piezoelectric response of single-crystal tetragonal BT has been demonstrated either due to the formation of engineered domain walls[39] or due to Ti−O bond oscillations.[40] Since we observe the occurrence of all the characteristic relaxor phenomena from DSC and dielectric measurements, it supports the ferroelectric relaxor behavior of BT nanoparticles.

To further demonstrate the ability to polarize the BT nanoparticles in the ferroelectric phase (ability to electrically write and read), Kelvin-probe/surface potential microscopy (SPM) was used (Figure 4).[5] Initially, a DC bias voltage of +4 V (V_{write}) was applied between the conductive AFM tip and the BT particles that results in orientation of local electric dipoles of BT particles, following which spontaneous polarization of BT particles was recorded (V_{read}) in the form of potential/voltage signals using SPM. This electrical information is evident in the form of brighter-contrasting elevations in Figure 4, A and C. Similarly, when a DC bias voltage $V_{write} = -4$ V was applied between the tip and the particles, it results in orientation of local electric dipoles of BT particles in direction opposite to that of +4V bias, following which recorded spontaneous polarization (V_{read}) of BT particles is evident in the form of darker-contrasting depressions observed in Figure 4, B and D. This change in image contrast due to reversal of electrical polarization of BT particles on reversal of external DC bias voltage suggests the ferroelectric nature of BT nanoparticles synthesized using fungus-mediated biological route. It was noted that when a DC bias voltage of <4 V was applied, significant contrast could not be observed in voltage images; however, administration of ≥4 V DC bias voltage results in increasing contrast in voltage images, hence, resulting in fusion of electrical signals arising from individual BT particles (data not shown).

In another experiment, to demonstrate the selective polarizability of BT particles in various regions of a single substrate, DC bias voltages (V_{write}) of +4 , 0, and −4 V were sequentially applied between the conductive AFM tip and BT particles in a single scan. This results in polarization of electric domains in various directions in different regions of the substrate in response to diverse applied voltages. While reading the electric information (V_{read}) using SPM, it is evident that application of +4 V bias results in brighter contrast signals from BT particles, 0 V bias does not show any potential signals, and −4V bias results in darker contrast signals from BT particles (Figure 4E), which suggest that the BT particles can be selectively written and read on a single substrate. A topography image of BT particles was also recorded for the same region as is evident from Figure 4F. Thus, SPM imaging clearly demonstrates that the room-temperature synthesized BT nanoparticles possess ferroelectric property in response to the applied external electric field and the various particles can be selectively written and read using SPM.

The presence of a room-temperature tetragonal phase in sub-10 nm BT nanoparticles, responsible for their ferroelectric behavior, is quite interesting and, at least to our knowledge, has not been reported previously. However, there are considerable discrepancies in the reported boundary sizes between the cubic and tetragonal phases, which vary from 190[37] to about 30 nm.[41] According to a surface effect model proposed by Yen and co-workers in terms of crystallite size effect, excess surface energy associated with ultrafine particles has been found to be responsible for the stabilization of the high-temperature cubic phase at room temperature for particles about 30 nm in size. Conversely, in our study, we do not observe stabilization of high-temperature cubic phase even in sub-10 nm particles, and these particles exhibit tetragonality at room temperature. We believe that the charged biomolecules associated with sub-10 nm BT particles might be playing an important role in avoiding

(39) Wada, S.; Suzuki, S.; Noma, T.; Suzuki, T.; Osada, M.; Kakihana, M.; Park, S. E.; Cross, L. E.; Shrout, T. R. *Jpn. J. Appl. Phys.* **1999**, *38*, 5505.
(40) Simon, A.; Ravez, J.; Maglione, M. *J. Phys.: Condens. Matter* **2004**, *16*, 963.
(41) Yen, F. S.; Chang, C. T.; Chang, Y. H. *J. Am. Ceram. Soc.* **1990**, *73*, 3422.
(42) Gao, Y.; Masuda, Y.; Yonezawa, T.; Koumota, K. *Chem. Mater.* **2002**, *14*, 5006.
(43) Gass, J.; Poddar, P.; Almand, J.; Srinath, S.; Srikanth, H. *Adv. Funct. Mater.* **2006**, *16*, 71.

the stabilization of the cubic phase by balancing for excess surface energy in ultrafine particles and hence resulting in a room-temperature tetragonal phase. It is worth mentioning that cationic proteins have been found to be associated with previously synthesized oxide nanoparticles using biological routes.[18−25]

Conclusion

The presence of a room-temperature ferroelectric phase in BT nanoparticles below 10 nm has significant importance as it opens up new opportunities such as ultrahigh density nonvolatile ferroelectric memories, ultrasmall capacitors, etc. While reduction in the bit size in the traditional ferromagnetic memories by reducing the particle size below 10 nm causes unstable behavior due to the superparamagnetism, we believe that the demonstration of the ferroelectricity in such a small size may revolutionize the electronics industries. In conclusion, we have shown here a fungus-mediated biological route toward the synthesis of tetragonal barium titanate nanoparticles of sub-10 nm dimensions under ambient conditions. The extracellular proteins synthesized by the fungus are believed to provide a hydrolyzing as well as a confining template for the synthesis of nanoscale BT particles, as reported previously for binary oxide nanoparticles.[22−25] The exact biochemical role of these proteins in fungal metabolism is under investigation. Moreover, the Curie transition behavior and ferroelectric response of 4−8 nm BT nanoparticles has also been demonstrated. Using microorganisms for the room-temperature synthesis of ternary oxide nanomaterials such as $BaTiO_3$ is an exciting possibility and could lead to ecofriendly and economically viable methods for the synthesis of complex oxide nanomaterials of technological interest.

Acknowledgment. V.B. thanks Council of Scientific and Industrial Research (CSIR) for a research fellowship. We acknowledge the Department of Science and Technology for setting up a unit on Nanoscience and Technology (DST-UNANST) at NCL, Pune, India. Contributions of Dr. P. V. Satyam (IoP, Bhubneshwar) for HR-TEM imaging, Ms. Minakshi Chaudhary (NCL, Pune) for AFM measurements, Mr. Anil Jadhav (NCL, Pune) for simulation of XRD data, Dr. K. Vijaymohanan and Mrs. Sneha A. Kulkarni (NCL, Pune) for frequency-dependent dielectric measurements, Dr. C. Ramesh (Polymer Chemistry, NCL Pune) for temperature-dependent XRD studies, and Mr. H. Muthurajan (ARDE, Pune) for temperature-dependent dielectric measurements are also acknowledged.

Supporting Information Available: Thermogravimetric analysis of BT nanoparticles synthesized using fungus *F. oxysporum* before and after their calcination (S1). FT-IR and AFM analysis of BT−PMMA nanocomposites (S2). This material is available free of charge via the Internet at http://pubs.acs.org.

JA063011M